Field and Temperature Dependence of the Skyrmion Lattice Phase in Chiral Magnet Membranes

David M. Burn,[1] Shasha Wang,[2] Weiwei Wang,[3] Gerrit van der Laan,[1,*] Shilei Zhang,[4,5,†] Haifeng Du,[2,‡] and Thorsten Hesjedal[6,§]

[1] *Magnetic Spectroscopy Group, Diamond Light Source, Didcot OX11 0DE, United Kingdom*
[2] *High Magnetic Field Laboratory, Chinese Academy of Sciences, Hefei 230031, China*
[3] *Institutes of Physical Science and Information Technology, Anhui University, Hefei 230601, China*
[4] *School of Physical Science and Technology, ShanghaiTech University, Shanghai 201210, China*
[5] *ShanghaiTech Laboratory for Topological Physics, ShanghaiTech University, Shanghai 200031, China*
[6] *Clarendon Laboratory, Department of Physics, University of Oxford, Parks Road, Oxford, OX1 3PU, United Kingdom*

(Dated: January 12, 2020)

Magnetic skyrmions are nanosized magnetization whirls that exhibit topological robustness and nontrivial magnetoelectrical properties, such as emergent electromagnetism and intriguing spin dynamics in the microwave-frequency region. In chiral magnets, skyrmions are usually found at a pocket in the phase diagram in the vicinity of the ordering temperature, wherein they order in the form of a hexagonal skyrmion lattice (SkL). It is generally believed that this equilibrium SkL phase is a uniform, long-range-ordered magnetic structure with a well-defined lattice constant. Here, using high-resolution small angle resonant elastic x-ray scattering, we study the field- and temperature-dependence of the skyrmion lattice in FeGe and Cu_2OSeO_3 membranes. Indeed, Cu_2OSeO_3 shows the expected rigid skyrmion lattice, known from bulk samples, that is unaffected by tuning field and temperature within the phase pocket. In stark contrast, the lattice constant and skyrmion size in FeGe membranes undergo a continuous evolution within the skyrmion phase pocket, whereby the lattice constant changes by up to 15% and the magnetic scattering intensity varies significantly. Using micromagnetic modeling, it is found that for FeGe the competing energy terms contributing to the formation of the skyrmion lattice fully explain this breathing behavior. In contrast, for Cu_2OSeO_3 this stabilizing energy balance is less affected by the smaller field variation across the skyrmion pocket, leading to the observed rigid lattice structure.

I. INTRODUCTION

Exploiting topological properties of quantum materials for commercial applications has been a central topic for nanoscience and nanotechnology in recent years. Topologically ordered magnetic systems, such as magnetic solitons [1, 2], vortices [3], skyrmions [4, 5] and Hopfions [6], have nontrivial magnetization configurations in real space which exhibit robustness against perturbations and defects. This makes them excellent candidates for binary information carriers [4]. Among them, magnetic skyrmions are particularly promising as they exist in many materials systems [7–16], and host a number of novel effects, such as emergent electromagnetism [17, 18] and nonreciprocal microwave response [19]. They can be generated, annihilated, and manipulated with ease, making them suitable for future for spintronics applications [4].

Magnetic skyrmions were first experimentally discovered in noncentrosymmetric transition-metal compounds, such as MnSi [7], FeCoSi [8], FeGe [9], Cu_2OSeO_3 [10], CoZnMn [11], and others. In these materials, skyrmions have a delicate spin arrangement which is usually governed by the balance of the energy terms of the system [20]. On a microscopic scale, the skyrmion texture is characterized by the topological winding number [4, 21], radial profile [4], chirality, polarity, and helicity angle [22, 23]. On a mesoscopic scale, skyrmions with winding number $N = 1$ can display different shape (commonly either hexagonal or circular depending on their radial profile), size, and correlation length [24], and it is the mesoscopic properties that determine most of their merits for applications [4, 24].

In noncentrosymmetric helimagnets, the most intensively studied skyrmion order is the equilibrium skyrmion lattice (SkL) phase [7–11], which exists in a small phase pocket in the temperature-field phase diagram close to the transition temperature (T_C). A 'universal' theoretical framework has been successfully applied to treat the physics of the SkL phase [25]. In short, within this micromagnetic model, the competition between exchange stiffness, Dzyaloshinskii-Moriya interaction (DMI) and Zeeman energy favors noncollinear chiral modulations. With the further contribution of thermal fluctuations [7], and/or anisotropy [20], and/or surface confinement [22, 26, 27], the long-range ordered SkL phase can be stabilized. Within this framework, both the skyrmion size and SkL lattice constant are determined by the ratio

* Gerrit.vanderLaan@diamond.ac.uk
† zhangshl1@shanghaitech.edu.cn
‡ duhf@hmfl.ac.cn
§ Thorsten.Hesjedal@physics.ox.ac.uk

of the strength of exchange interaction and DMI. Therefore, for any parameter set within the equilibrium SkL phase, it is commonly believed that the skyrmions are uniformly ordered, i.e., with a fixed size and correlation length [4, 25, 28]. This model is indeed in agreement with many small-angle neutron scattering (SANS) studies on bulk samples [29] and real-space magnetic imaging studies on thin membranes [8, 10, 30].

For future skyrmion device applications, the behavior of skyrmions in confined geometries, such as thin films, is of key importance. Interestingly, in a thinned-down helimagnet specimen with a thickness comparable to the characteristic modulation pitch of the helix, the SkL phase pocket can be extended [9, 10, 31] due to additional anisotropy [4, 32] and instabilities induced by the surface [26]. Despite of the extension of the phase pocket, the skyrmion lattice constant and individual skyrmion size are generally believed to remain the same in FeGe [9], MnSi [31], and Cu_2OSeO_3 [10] samples with confined geometries. In fact, the skyrmion lattice constant is nearly identical to the helical modulation period λ, which results from a competition between exchange interaction and DMI [33].

Recently, additional skyrmion phases were discovered, namely, a low-temperature skyrmion phase [28] and metastable skyrmion states [34–36]. In the former case, enhanced cubic anisotropy at temperatures far below T_C encourages skyrmions to nucleate, competing against the conical order [28]. In such a scenario, the skyrmion phase lacks long-range order, and the correlation length increases as a function of field, resulting from the rivaling anisotropy energy. In the latter case, the metastable skyrmion state, produced by field-cooling from the equilibrium SkL state [37, 38], also undergoes systematic size and correlation variations, i.e., by increasing the magnetic field, the skyrmion size monotonically decreases, while the lattice constant monotonically increases [30]. This is in the case that the direction of the field is aligned with the magnetization separating the skyrmions, and antiparallel with the magnetization in the center of the skyrmion. Further, a Lorentz transmission electron microscopy study by McGrouther *et al.* has found the field- and film thickness-dependent evolution of the SkL phase in FeGe [39], in contrast to previous reports [9].

Here, using high-resolution small angle resonant elastic x-ray scattering (SAREXS) on membranes [40–43], we carried out a comparative study of the SkL phase in the chiral magnets FeGe and Cu_2OSeO_3. Whereas Cu_2OSeO_3 shows a rigid SkL, in agreement with the general assumptions of the 'universal' skyrmion model, we find a continuously varying SkL phase in FeGe membranes in agreement with an earlier LTEM study [39]. SAREXS is particularly suited for studying the small changes of the reciprocal space SkL propagation wavevectors due to two reasons: First, synchrotron-produced soft x-rays are highly monochromatic (photon energy $\Delta E < 0.1\,\mathrm{eV}$), thereby greatly restricting the conditions under which the Bragg condition for magnetic diffraction is met [21, 44–48]. Second, the distance between the sample and the CCD camera can be comparably large (474 mm in our case), leading to an angular resolution of 0.0016°. Consequently, the resolution in reciprocal space vector $\mathbf{q}$ reaches 1.6×10^{-5} nm^{-1} at the Fe L_3 edge (and 1.2×10^{-5} nm^{-1} at the Cu L_3 edge), making it possible to study very small momentum transfers in magnetic diffraction. Surprisingly, we find a non-monotonic evolution of the SkL constant λ within the equilibrium SkL phase in FeGe membranes, and a rigid lattice in identically prepared Cu_2OSeO_3 membranes. In FeGe, either by increasing temperature or field, λ first decreases, and consecutively increases, before entering into a different magnetic phase. Supported by micromagnetic simulations, it is confirmed that the skyrmion diameter d in FeGe also changes accordingly. The behavior of FeGe is fundamentally different from that of Cu_2OSeO_3, as well as from the recently reported metastable skyrmion state in FeGe [30].

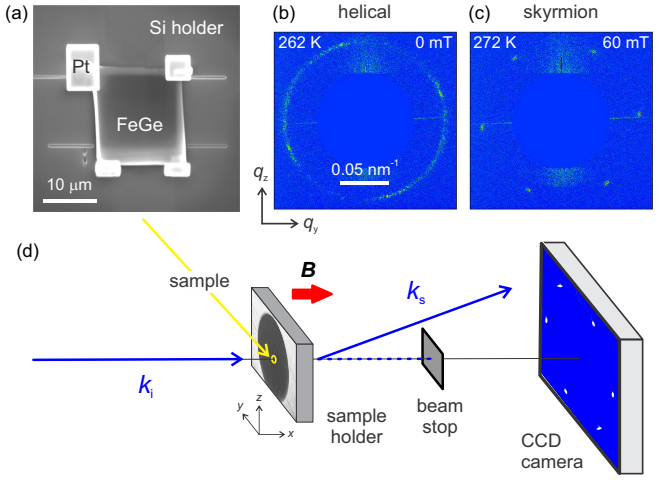

FIG. 1. Small angle resonant elastic x-ray scattering setup. (a) Scanning electron micrograph of the 200-nm-thick FeGe membrane, mounted on a 3-mm-diameter Si holder with a 10×10 μm^2 aperture using Pt (the 162-nm-thick Cu_2OSeO_3 membrane is not shown). (b) Typical magnetic scattering patterns obtained in the helical and (c) skyrmion lattice phase of FeGe. (d) The incident x-rays (wavenumber k_i) are scattered under small angles (k_s) and their intensity distribution is detected using a CCD camera. A beam stop is used to block the straight-through beam, enhancing the contrast of the scattered x-rays. The magnetic field is applied out-of-plane (along the beam direction). The energy of the circularly polarized x-rays was tuned to the Fe and Cu L_3 edges, respectively. The temperature of the sample can be controlled in the range from 10 to 400 K.

II. EXPERIMENTAL DETAILS

The SAREXS studies were carried out on FeGe and Cu_2OSeO_3 membranes in transmission geometry on beamline I10 at the Diamond Light Source (Oxfordshire,

UK). Circularly polarized x-rays with energy tuned to the Fe and Cu L_3 edges were scattered by the magnetic structure of the sample. The small angle scattering was captured by a CCD detector with a sample-detector distance of 474 mm. The 200-nm-thick FeGe and the 162-nm-thick Cu_2OSeO_3 membranes, measuring $20 \times 20\,\mu m^2$ in area, were milled from FeGe and Cu_2OSeO_3 single crystals using focused-ion beam processing. The membranes were transferred to a 3-mm-diameter Si holder with a $10 \times 10\,\mu m^2$ square aperture in the center, and secured in place with Pt. The strain in our samples was minimized by using the mounting method shown in Fig. 1(a) (also see Ref. [42]), in stark contrast to the deliberately strained FeGe plates investigated by Shibata *et al.* [49]. Note that the transition temperatures in thin plates generally deviate from the respective bulk values, not necessarily owing to strain, but very strongly depending on sample geometry (thickness and shape) [9].

The samples were mounted in the Portable Octupole Magnet System (POMS) on a He cryostat within the 3D vector magnet, and the small angle magnetic scattering was investigated as a function of both temperature and magnetic field applied out-of-plane, i.e., along the beam direction, as shown in Fig. 1(d). Representative scattering patterns obtained for helical and SkL phase of FeGe are shown in Figs. 1(b) and 1(c), respectively. The helical phase SAREXS pattern, obtained at zero field and 262 K, is characterized by a ring-shaped intensity distribution due to disorder. A weak four-fold symmetry is apparent in Fig. 1(b) as well, indicative of two helical domains locked in two perpendicular in-plane directions due to the magnetocrystalline anisotropy. Figure 1(c) shows the expected six-fold symmetric pattern stemming from a well-ordered skyrmion lattice state (for FeGe obtained at 272 K and 60 mT).

A graphics processor unit (GPU)-supported finite-difference micromagnetic package JuMag [50] was used to investigate the skyrmion lattice phase. The minimal model follows the work of Leonov *et al.* [27] and only includes exchange energy, DMI, and Zeeman energy. The energy of the system is minimized using a gradient descent method where the step-size is chosen according to the Barzilai-Borwein rule. To determine the skyrmion lattice constant at which the system has lowest energy density, the total number of discretization cells was fixed to be 460, 478, and 1 in x, y, and z, respectively, and the cell size (dx and dy range from 0.8 nm to 1.1 nm, whereas dz is fixed to 2 nm) was varied for each external field value. The used parameters for FeGe are the saturation magnetization $M_s = 3.84 \times 10^5$ A/m, exchange stiffness constant $A = 8.78 \times 10^{-12}$ J/m, and DMI constant $D = 1.58 \times 10^{-3}$ J/m^2 [51]. For Cu_2OSeO_3 the following parameters were used [52]: $M_s = 1.044 \times 10^5$ A/m, $A = 3.547 \times 10^{-13}$ J/m, $D = 7.43 \times 10^{-5}$ J/m^2. Two-dimensional periodic boundary conditions are used (whereas the demagnetization energy is ignored). It is worth noting that in very thin samples (as considered here), the confined geometry may amplify the demagnetization effect, from which skyrmions may be favored to exist with modified size.

III. RESULTS AND DISCUSSION

A. Magnetic phase diagrams

Magnetic scattering patterns were obtained as a function of field at various temperatures. Figures 2(a) and 2(b) illustrate the evolution of the SAREXS SkL patterns as a function of field for FeGe (at 257 K) and Cu_2OSeO_3 (at 44 K), respectively. Here, the change in $\mathbf{q}$ when entering the skyrmion phase can be seen with reference to the dashed circles which indicate the $\mathbf{q}$ obtained from the zero field disordered helical state (at zero field). For FeGe, at 96 mT, $\mathbf{q}$ in the skyrmion state is initially small. With increasing field, $\mathbf{q}$ expands to its maximum at 148 mT before a significant reduction occurs towards higher fields (data shown for 168 and 192 mT). In stark contrast, for Cu_2OSeO_3 $\mathbf{q}$ only reduces slightly when entering the skyrmion phase (see six-fold pattern for 28 mT). This initial $\mathbf{q}$ remains constant throughout the skyrmion phase. Images are shown up to a field of 40 mT, above which the system starts to leave the skyrmion pocket.

Magnetic phase diagrams were determined for FeGe as field-temperature maps showing the scattered intensity and the magnitude of the magnetic scattering vector, $|\mathbf{q}|$ in Figs. 3(a) and 3(b), respectively. These were obtained from the scattering patterns [example shown in Fig. 2] by first integrating in rings to obtain the scattered intensity as a function of $|\mathbf{q}|$. Note that this analysis includes all ordered skyrmions (single- and multi-domain), and excludes other magnetically ordered phases, such as the helical or conical phase, which can be distinguished by their unique scattering patterns and different $\mathbf{q}$ values. A Lorentzian was fitted for each image, parameterized by a peak position, intensity, and width. The intensity and peak position $|\mathbf{q}|$ are shown in Figs. 3(a) and 3(b), respectively. Two clear pockets of strong scattered intensity are shown in Fig. 3(a) which correspond to the helical (Hel) and skyrmion (SkL) magnetic phases. These pockets extend up to $T_C \approx 273$ K and to the upper critical field, H_{C2}, beyond which the scattered intensity vanishes for the ferromagnetic phase. For Cu_2OSeO_3, due to the constant $|\mathbf{q}|$, such an analysis is obviously not possible. A magnetic phase diagram, obtained by measurements in reflection, can be found in Ref. [45].

Figure 3(b) shows the corresponding variations in $|\mathbf{q}|$ for FeGe across the phase diagram where a scattered intensity can be measured above the noise level. Significant changes in $|\mathbf{q}|$ are observed across each phase pocket. In particular, for the skyrmion phase, the maximum $|\mathbf{q}|$ is found for magnetic fields in the center of the phase pocket with a decrease in $|\mathbf{q}|$ observed for both higher and lower fields. Furthermore, this maximum $|\mathbf{q}|$ also increases as a function of temperature, reaching a maximum just below

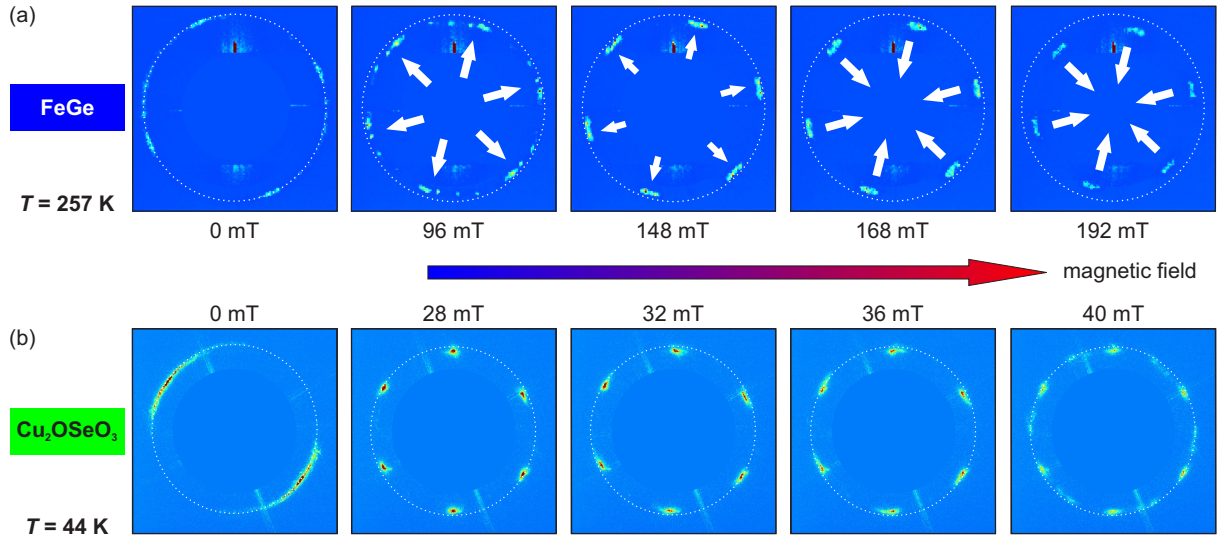

FIG. 2. Magnetic scattering patterns for (a) FeGe and (b) Cu_2OSeO_3. (a) FeGe for different fields at 257 K. In zero field, the disordered helical phase can be seen, for which **q** is maximal (as indicated by a dashed circle). Increasing the field towards 100 mT, the system is driven into the SkL phase showing a six-fold symmetric scattering pattern. The appearance of several six-fold sets is indicative of a multidomain state. Increasing the field further results in an increase in **q** until a maximum is reached at ∼148 mT before a considerable shrinking in **q** towards the border of the SkL pocket at higher fields. The white arrows in the images illustrate the trend in **q** as the field is increased. (b) Cu_2OSeO_3 for different fields at 44 K. As above, the dashed circle indicates the disordered helical phase with maximal **q** (in zero field). Upon entering the SkL phase (∼25 mT), six diffraction peaks are clearly visible, with a **q** slightly lower than in the helical phase. This **q** remains constant throughout the SkL phase pocket.

T_C. The helical phase also shows a decrease in $|\mathbf{q}|$ with an increase in magnetic field but with a negligible temperature dependence. Figure 3(c) shows cuts through the phase diagram at constant fields as indicated. The transition temperature is at its maximum for the lowest field value that stabilizes the skyrmion phase, and decreases with increasing field.

B. Temperature- and Field-Dependence of q for FeGe

The evolution of $|\mathbf{q}|$ for FeGe as a function of magnetic field at five selected temperatures is shown in Fig. 4. The helical phase present at lower fields has a $|\mathbf{q}|$ that decreases with increasing field, accompanied by a loss in scattered intensity [53]. For temperatures above 251 K, Figs. 4(b)–4(e) also show the skyrmion phase with a more complex $|\mathbf{q}|$ dependence. With increasing field, $|\mathbf{q}|$ first increases to a maximum before a more rapid decrease occurs with a loss in scattered intensity towards the upper critical field. This change in $|\mathbf{q}|$ appears as a characteristic crescent-like feature, which is most pronounced at 257 K [Fig. 4(c)] where $|\mathbf{q}|$ changes with increasing field from 0.85 to 0.90, and down to 0.80 nm^{-1}. The largest change in $|\mathbf{q}|$ of 15% was observed at 268 K [Fig. 4(d)]. Comparing the panels in Fig. 4, the crescent-shaped features shift towards lower fields as the temperature is increased. This behavior is trivial and can be revealed by rescaling the applied field by the upper critical field for each temperature. As a function of this reduced field, the crescent shapes line up with each other, as shown in Fig. 3 in Ref. [53], and they appear to be almost flat (i.e., field-independent) in the middle of the skyrmion pocket. Note that the maximum $|\mathbf{q}|$ in the skyrmion phase increases as the temperature is increased.

C. Micromagnetic Simulations

Standard micromagnetic simulations were performed to calculate the skyrmion lattice in thin films by minimizing the system's energy following the approach of Leonov *et al.* [27]. Figure 5 shows on the left the simulated real-space skyrmion lattice and on the right the corresponding simulated SAREXS patterns for FeGe [46]. The distances between the skyrmion centers in Figs. 5(a)–5(c) are 85.6, 82.8, and 94.8 nm, respectively, for applied fields of 60, 140, and 270 mT. The corresponding simulated SAREXS intensities are shown in Figs. 5(d)–5(f); $|\mathbf{q}|$ has its maximum value for an applied field of 140 mT. The crescent-shaped $|\mathbf{q}|(B)$ behavior is qualitatively well reproduced by the simulations with $|\mathbf{q}|$ first expanding before undergoing a more rapid contraction with increasing field. Our findings are in agreement with previous theoretical studies [54–56], and complement the Lorentz transmission electron microscopy based study on membranes by McGrouther *et al.* [39].

For Cu_2OSeO_3, the simulations shown in Fig. 6 con-

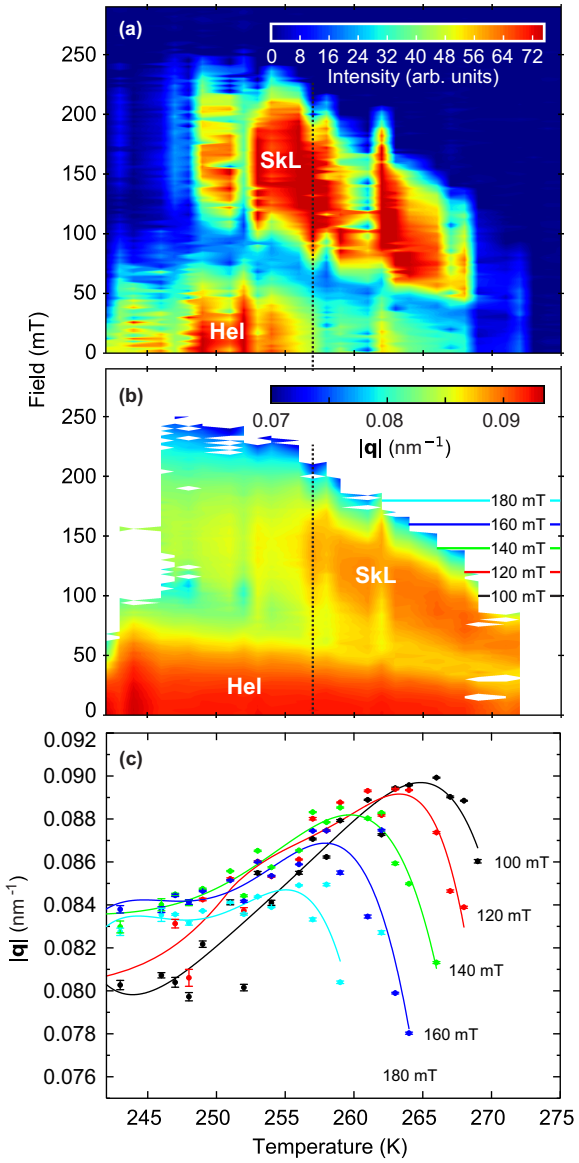

FIG. 3. Magnetic phase diagrams for FeGe. Maps of (a) the scattered intensity, and (b), the magnitude of the magnetic scattering vector **q** as a function of temperature and magnetic field. Pockets representing the helical (Hel) and skyrmion lattice phase (SkL) are labeled and above $T_C \approx 273\,K$ the magnetic intensity vanishes. (c) Constant field cuts through the phase diagram showing the temperature-dependent evolution of $|\mathbf{q}|$.

firm that within the experimentally determined skyrmion phase pocket reaching from 20 to 40 mT, $|\mathbf{q}|$ remains constant. On the other hand, in the transition region from the skyrmion to the conical phase at high fields, in which both phases may coexist, the skyrmion lattice constant is indeed increasing, analogous to FeGe. We find that the addition of a cubic anisotropy term has only negligible effects on the behavior of Cu_2OSeO_3. Note that the $|\mathbf{q}|$ values obtained by micromagnetic simulations using the minimal model deviate from the experimental values as, e.g., demagnetization has not been taken into account. Also, for a quantitative agreement, effective materials constants have to be used.

D. Discussion

For FeGe, at low fields, the individual skyrmions are large, occupying the majority of the unit cell within the lattice. The skyrmions therefore sense the boundary and adopt the six-fold symmetry of the lattice. With an increase in field, the size of skyrmions shrinks in order to minimize the Zeeman energy contribution from spins not aligned with the applied field [55]. As a result, the skyrmions are now radial symmetric and smaller than the unit cell. This shrinking of the skyrmion reduces the constraint on the size of the lattice, i.e., the lattice parameter shrinks and $|\mathbf{q}|$ increases. In contrast, skyrmions in MnGe which form a square lattice with a different symmetry [54], show a period that is independent of the applied field [57].

With a further increase in field, the FeGe skyrmion lattice constant increases, driven by the relative dominance of the Zeeman energy over the DMI and exchange energy contributions, as shown in Fig. 7. This leads to smaller skyrmions surrounded by larger areas of field-aligned spins. In other words, the lattice parameter is in part limited by the size of the skyrmion, which depends on the relative orientation of the field and the magnetization in the center of the skyrmion. When both are parallel, the spin alignment in the center is favored, thus increasing the radius of the skyrmion and vice versa [54]. For very high fields, this eventually leads to the breakup of the SkL lattice and its transformation into a set of isolated repulsive skyrmions, as described in earlier theoretical studies [54, 55]. Note that our scattering measurement is not sensitive to single or unordered skyrmions, which also excludes the study of precursor phenomena in this area of the phase diagram [58].

The discrepancy between the behavior of FeGe and that of Cu_2OSeO_3, i.e., the absence of skyrmion lattice breathing, may well be due to the smaller relative field range of the skyrmion pocket. Whereas for FeGe the field roughly doubles across the pocket, it only changes from ∼28 to 40 mT in case of Cu_2OSeO_3. From the micromagnetic simulation it becomes clear that the biggest change is to be expected for higher fields close to the boundary of the skyrmion pocket, which is however a mixed phase region in case of Cu_2OSeO_3. Finally, we would like to emphasize that the observed effects, although most likely present near the surface in bulk samples, will not be picked up by volume-averaging techniques like SANS.

IV. CONCLUSIONS

In summary, we have studied the field- and temperature-dependence of the reciprocal lattice vector

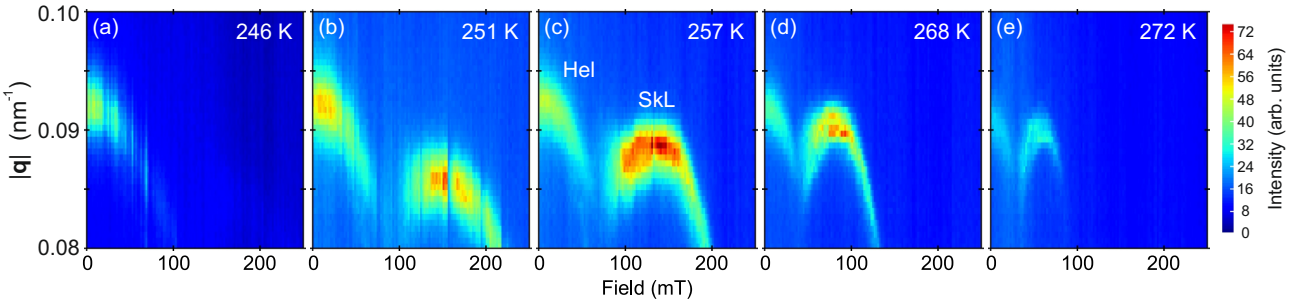

FIG. 4. Evolution of the magnetic scattering vector $|\mathbf{q}|$ for FeGe as a function of field and temperature. Plots of the scattered intensity as a function of both $|\mathbf{q}|$ and magnetic field showing the field dependence of $|\mathbf{q}|$ for both the helical phase at low fields and the skyrmion lattice phase towards higher fields. (a) At low temperatures (246 K) only the helical phase can be seen with a $|\mathbf{q}|$ that reduces with increasing field until the phase vanishes above ∼100 mT. (b-e) At higher temperatures, ≥251 K, the SkL phase appears with a $|\mathbf{q}|$ that first increases to a maximum followed by a sharper decline with increasing fields. This crescent-shaped feature is most pronounced at 257 K in (c). Both phases coexist up to T_C.

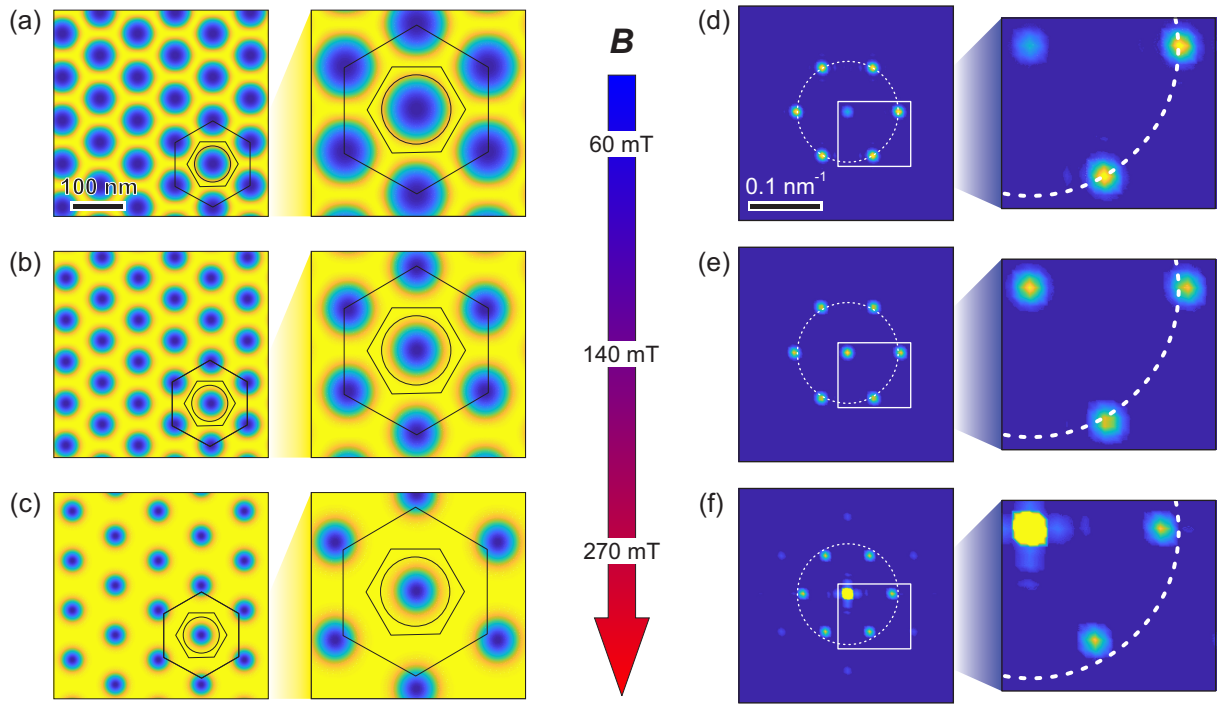

FIG. 5. Micromagnetic simulations: Real-space skyrmion lattice and SAREXS patterns for FeGe. Micromagnetic simulations of the real-space (a,b,c) and the derived SAREXS intensities (d,e,f) for the SkL in an out-of-plane field of 60, 140, and 270 mT respectively. Close-ups in the adjacent rows illustrate clearly a monotonic decrease in skyrmion size with applied field despite an initial shrinking of the SkL lattice constant between 60 to 140 mT followed by a subsequent expansion at 270 mT. The SAREXS patterns show a consistent increase followed by a decrease in $|\mathbf{q}|$. For comparison, in (a,b,c), the size of a single low-field skyrmion is indicated by a hexagon and a circle; and the lattice by a larger hexagon connecting the skyrmion centers. The dashed circle in (d,e,f) represents the maximum $|\mathbf{q}|$.

$\mathbf{q}$ of the SkL phase in FeGe and Cu_2OSeO_3 membranes using high-resolution small angle x-ray scattering. The SkL phase in Cu_2OSeO_3 shows a rigid skyrmion lattice with no detectable field and temperature dependence, in agreement with the common conception of the equilibrium SkL phase in chiral magnets. In stark contrast, in FeGe, $|\mathbf{q}|$ is strongly field and temperature dependent and shows a crescent-shaped variation which has been explained alongside micromagnetic simulations. At higher fields, the lattice parameter expands to the point where the skyrmion lattice breaks apart at the upper critical field. At lower fields, the shrinking of the lattice parameter becomes constrained by the increasing skyrmion size. Energy minimization within the skyrmion internal spin structure determines the energy balance of the system resulting in the increase in skyrmion size, forcing the lattice

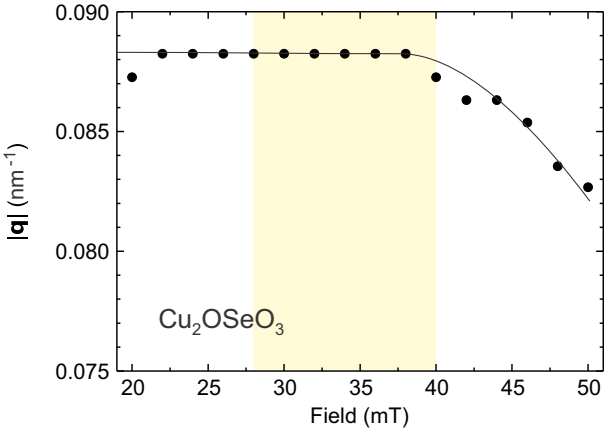

FIG. 6. Micromagnetic simulation results of the skyrmion lattice phase in Cu_2OSeO_3 at 44 K. Within the experimentally determined skyrmion phase pocket of ∼28 to 40 mT, the lattice constant indeed appears to be constant. For higher fields, $|\mathbf{q}|$ reduces as for the case of FeGe. The solid line is a guide to the eyes.

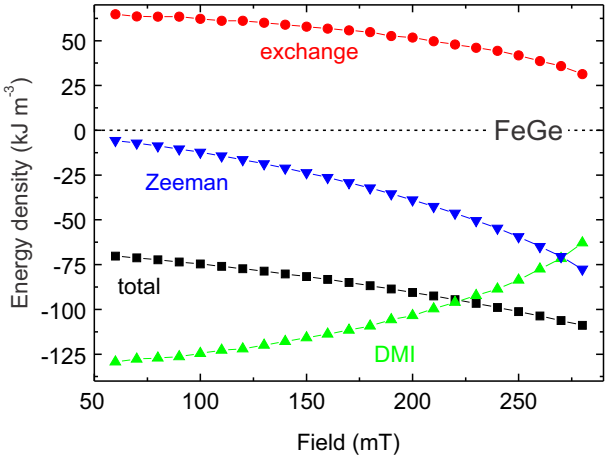

FIG. 7. Plot of the energy densities as a function of applied field. The total energy (black) is composed of exchange (red), Zeeman (blue), and DMI (green) terms.

parameter to increase again at lower fields. This mechanism is not yet active in Cu_2OSeO_3 due to the smaller extension of the skyrmion phase pocket. For the development of future spintronic applications, understanding the behavior of the individual skyrmions and the skyrmion lattice in chiral magnets in general is crucial. Our work highlights the importance of the fine energy balance in noncentrosymmetric chiral magnets, which is especially important for thin films and membranes.

ACKNOWLEDGMENTS

The SAREXS experiments were carried out using the portable octupole magnet system on beamline I10 at the Diamond Light Source (Oxfordshire, UK) under proposals SI20182 and SI20437. S.L.Z. acknowledges a starting grant from ShanghaiTech University. Financial support through the Engineering and Physical Sciences Research Council (EPSRC) under grant EP/N032128/1 is gratefully acknowledged.

[1] H.-B. Braun, Topological effects in nanomagnetism: From superparamagnetism to chiral quantum solitons, Adv. Phys. **61**, 1 (2012).
[2] Y. Togawa, T. Koyama, K. Takayanagi, S. Mori, Y. Kousaka, J. Akimitsu, S. Nishihara, K. Inoue, A. S. Ovchinnikov, and J. Kishine, Chiral magnetic soliton lattice on a chiral helimagnet, Phys. Rev. Lett. **108**, 107202 (2012).
[3] S. Komineas and N. Papanicolaou, Topology and dynamics in ferromagnetic media, Physica D **99**, 81 (1996).
[4] N. Nagaosa and Y. Tokura, Topological properties and dynamics of magnetic skyrmions, Nat. Nanotechnol. **8**, 899 (2013).
[5] F. Zheng, F. N. Rybakov, A. B. Borisov, D. Song, S. Wang, Z.-A. Li, H. Du, N. S. Kiselev, J. Caron, A. Kovács, M. Tian, Y. Zhang, S. Blügel, and R. E. Dunin-Borkowski, Experimental observation of chiral magnetic bobbers in B20-type FeGe, Nat. Nanotechnol. **13**, 451 (2018).
[6] P. J. Ackerman and I. I. Smalyukh, Static three-dimensional topological solitons in fluid chiral ferromagnets and colloids, Nat. Mater. **16**, 426 (2016).
[7] S. Mühlbauer, B. Binz, F. Jonietz, C. Pfleiderer, A. Rosch, A. Neubauer, R. Georgii, and P. Böni, Skyrmion lattice in a chiral magnet, Science **323**, 915 (2009).

[8] X. Z. Yu, Y. Onose, N. Kanazawa, J. H. Park, J. H. Han, Y. Matsui, N. Nagaosa, and Y. Tokura, Real-space observation of a two-dimensional skyrmion crystal, Nature **465**, 901 (2010).

[9] X. Z. Yu, N. Kanazawa, Y. Onose, K. Kimoto, W. Z. Zhang, S. Ishiwata, Y. Matsui, and Y. Tokura, Near room-temperature formation of a skyrmion crystal in thin-films of the helimagnet FeGe, Nat. Mater. **10**, 106 (2011).

[10] S. Seki, X. Z. Yu, S. Ishiwata, and Y. Tokura, Observation of skyrmions in a multiferroic material, Science **336**, 198 (2012).

[11] Y. Tokunaga, X. Z. Yu, J. S. White, H. M. Rønnow, D. Morikawa, Y. Taguchi, and Y. Tokura, A new class of chiral materials hosting magnetic skyrmions beyond room temperature, Nat. Commun. **6**, 7638 (2015).

[12] W. Jiang, P. Upadhyaya, W. Zhang, G. Yu, M. B. Jungfleisch, F. Y. Fradin, J. E. Pearson, Y. Tserkovnyak, K. L. Wang, O. Heinonen, S. G. E. te Velthuis, and A. Hoffmann, Blowing magnetic skyrmion bubbles, Science **349**, 283 (2015).

[13] O. Boulle, J. Vogel, H. Yang, S. Pizzini, D. de Souza Chaves, A. Locatelli, T. O. Mentes, A. Sala, L. D. Buda-Prejbeanu, O. Klein, M. Belmeguenai, Y. Roussigné, A. Stashkevich, S. M. Chérif, L. Aballe, M. Foerster, M. Chshiev, S. Auffret, I. M. Miron, and G. Gaudin, Room-temperature chiral magnetic skyrmions in ultrathin magnetic nanostructures, Nat. Nanotechnol. **11**, 449 (2016).

[14] S. Woo, K. Litzius, B. Krüger, M.-Y. Im, L. Caretta, K. Richter, M. Mann, A. Krone, R. M. Reeve, M. Weigand, P. Agrawal, I. Lemesh, M.-A. Mawass, P. Fischer, M. Kläui, and G. S. D. Beach, Observation of room-temperature magnetic skyrmions and their current-driven dynamics in ultrathin metallic ferromagnets, Nat. Mater. **15**, 501 (2016).

[15] C. Moreau-Luchaire, C. Moutafis, N. Reyren, J. Sampaio, C. A. F. Vaz, N. V. Horne, K. Bouzehouane, K. Garcia, C. Deranlot, P. Warnicke, P. Wohlhüter, J. M. George, M. Weigand, J. Raabe, V. Cros, and A. Fert, Additive interfacial chiral interaction in multilayers for stabilization of small individual skyrmions at room temperature, Nat. Nanotechnol. **11**, 444 (2016).

[16] A. Soumyanarayanan, M. Raju, A. L. Gonzalez Oyarce, A. K. C. Tan, M.-Y. Im, A. P. Petrović, P. Ho, K. H. Khoo, M. Tran, C. K. Gan, F. Ernult, and C. Panagopoulos, Tunable room-temperature magnetic skyrmions in Ir/Fe/Co/Pt multilayers, Nat. Mater. **16**, 898 (2017).

[17] J. Zang, M. Mostovoy, J. H. Han, and N. Nagaosa, Dynamics of skyrmion crystals in metallic thin films, Phys. Rev. Lett. **107**, 136804 (2011).

[18] T. Schulz, R. Ritz, A. Bauer, M. Halder, M. Wagner, C. Franz, C. Pfleiderer, K. Everschor, M. Garst, and A. Rosch, Emergent electrodynamics of skyrmions in a chiral magnet, Nat. Phys. **8**, 301 (2012).

[19] Y. Okamura, F. Kagawa, M. Mochizuki, M. Kubota, S. Seki, S. Ishiwata, M. Kawasaki, Y. Onose, and Y. Tokura, Microwave magnetoelectric effect via skyrmion resonance modes in a helimagnetic multiferroic, Nat. Commun. **4**, 2391 (2013).

[20] A. N. Bogdanov and D. A. Yablonskii, Thermodynamically stable 'vortices' in magnetically ordered crystals. the mixed state of magnets, Sov. Phys. JETP **68**, 101 (1989).

[21] S. L. Zhang, G. van der Laan, and T. Hesjedal, Direct experimental determination of the topological winding number of skyrmions in Cu_2OSeO_3, Nat. Commun. **8**, 14619 (2017).

[22] S. L. Zhang, G. van der Laan, W. W. Wang, A. Haghighirad, and T. Hesjedal, Direct observation of twisted surface skyrmions in bulk crystals, Phys. Rev. Lett. **120**, 227202 (2018).

[23] S. L. Zhang, G. van der Laan, J. Müller, L. Heinen, M. Garst, A. Bauer, H. Berger, C. Pfleiderer, and T. Hesjedal, Reciprocal space tomography of 3D skyrmion lattice order in a chiral magnet, Proc. Natl. Acad. Sci. U.S.A. **115**, 6386 (2018).

[24] R. Wiesendanger, Nanoscale magnetic skyrmions in metallic films and multilayers: A new twist for spintronics, Nat. Rev. Mater. **1**, 16044 (2016).

[25] A. Bauer and C. Pfleiderer, Generic aspects of skyrmion lattices in chiral magnets, in *Topological Structures in Ferroic Materials: Domain Walls, Vortices and Skyrmions* (Springer International Publishing, Cham, 2016) pp. 1–28.

[26] F. N. Rybakov, A. B. Borisov, and A. N. Bogdanov, Three-dimensional skyrmion states in thin films of cubic helimagnets, Phys. Rev. B **87**, 094424 (2013).

[27] A. O. Leonov, Y. Togawa, T. L. Monchesky, A. N. Bogdanov, J. Kishine, Y. Kousaka, M. Miyagawa, T. Koyama, J. Akimitsu, T. Koyama, K. Harada, S. Mori, D. McGrouther, R. Lamb, M. Krajnak, S. McVitie, R. L. Stamps, and K. Inoue, Chiral surface twists and skyrmion stability in nanolayers of cubic helimagnets, Phys. Rev. Lett. **117**, 087202 (2016).

[28] A. Chacon, L. Heinen, M. Halder, A. Bauer, W. Simeth, S. Mühlbauer, H. Berger, M. Garst, A. Rosch, and C. Pfleiderer, Observation of two independent skyrmion phases in a chiral magnetic material, Nat. Phys. **14**, 936 (2018).

[29] J. Zang, V. Cros, and A. Hoffmann, eds., *Topology in Magnetism* (Springer, 2018).

[30] X. Yu, D. Morikawa, T. Yokouchi, K. Shibata, N. Kanazawa, F. Kagawa, T. Arima, and Y. Tokura, Aggregation and collapse dynamics of skyrmions in a non-equilibrium state, Nat. Phys. **10**, 832 (2018).

[31] A. Tonomura, X. Z. Yu, K. Yanagisawa, T. Matsuda, Y. Onose, N. Kanazawa, H. S. Park, and Y. Tokura, Real-space observation of skyrmion lattice in helimagnet MnSi thin samples, Nano Lett. **12**, 1673 (2012).

[32] M. N. Wilson, A. B. Butenko, A. N. Bogdanov, and T. L. Monchesky, Chiral skyrmions in cubic helimagnet films: the role of uniaxial anisotropy, Phys. Rev. B **89**, 094411 (2014).

[33] N. Kanazawa, Y. Onose, T. Arima, D. Okuyama, K. Ohoyama, S. Wakimoto, K. Kakurai, S. Ishiwata, and Y. Tokura, Large topological hall effect in a short-period helimagnet MnGe, Phys. Rev. Lett. **106**, 156603 (2011).

[34] P. Milde, D. Köhler, J. Seidel, L. M. Eng, A. Bauer, A. Chacon, J. Kindervater, S. Mühlbauer, C. Pfleiderer, S. Buhrandt, C. Schütte, and A. Rosch, Unwinding of a skyrmion lattice by magnetic monopoles, Science **340**, 1076 (2013).

[35] H. Oike, A. Kikkawa, N. Kanazawa, Y. Taguchi, M. Kawasaki, Y. Tokura, and F. Kagawa, Interplay between topological and thermodynamic stability in a metastable magnetic skyrmion lattice, Nat. Phys. **12**, 62 (2016).

[36] T. Nakajima, H. Oike, A. Kikkawa, E. P. Gilbert, N. Booth, K. Kakurai, Y. Taguchi, Y. Tokura, F. Kagawa, and T. h. Arima, Skyrmion lattice structural transition in MnSi, Sci. Adv. **3**, e1602562 (2017).

[37] H. Du, R. Che, L. Kong, X. Zhao, C. Jin, C. Wang, J. Yang, W. Ning, R. Li, C. Jin, X. Chen, J. Zang, Y. Zhang, and M. Tian, Edge-mediated skyrmion chain and its collective dynamics in a confined geometry, Nat. Commun. **6**, 8504 (2015).

[38] C. Jin, Z.-A. Li, A. Kovács, J. Caron, F. Zheng, F. N. Rybakov, N. S. Kiselev, H. Du, S. Blügel, M. Tian, Y. Zhang, M. Farle, and R. E. Dunin-Borkowski, Control of morphology and formation of highly geometrically confined magnetic skyrmions, Nat. Commun. **8**, 15569 (2017).

[39] D. McGrouther, R. J. Lamb, M. Krajnak, S. McFadzean, S. McVitie, R. L. Stamps, A. O. Leonov, A. N. Bogdanov, and Y. Togawa, Internal structure of hexagonal skyrmion lattices in cubic helimagnets, New J. Phys. **18**, 095004 (2016).

[40] Y. Yamasaki, D. Morikawa, T. Honda, H. Nakao, Y. Murakami, N. Kanazawa, M. Kawasaki, T. Arima, and Y. Tokura, Dynamical process of skyrmion-helical magnetic transformation of the chiral-lattice magnet FeGe probed by small-angle resonant soft x-ray scattering, Phys. Rev. B **92**, 220421 (2015).

[41] Y. Okamura, Y. Yamasaki, D. Morikawa, T. Honda, V. Ukleev, H. Nakao, Y. Murakami, K. Shibata, F. Kagawa, S. Seki, T. Arima, and Y. Tokura, Directional electric-field induced transformation from skyrmion lattice to distinct helices in multiferroic Cu_2OSeO_3, Phys. Rev. B **95**, 184411 (2017).

[42] Y. Okamura, Y. Yamasaki, D. Morikawa, T. Honda, V. Ukleev, H. Nakao, Y. Murakami, K. Shibata, F. Kagawa, S. Seki, T. Arima, and Y. Tokura, Emergence and magnetic-field variation of chiral-soliton lattice and skyrmion lattice in the strained helimagnet Cu_2OSeO_3, Phys. Rev. B **96**, 174417 (2017).

[43] V. Ukleev, Y. Yamasaki, D. Morikawa, K. Karube, K. Shibata, Y. Tokunaga, Y. Okamura, K. Amemiya, M. Valvidares, H. Nakao, Y. Taguchi, Y. Tokura, and T. Arima, Element-specific soft x-ray spectroscopy, scattering, and imaging studies of the skyrmion-hosting compound $Co_8Zn_8Mn_4$, Phys. Rev. B **99**, 144408 (2019).

[44] S. L. Zhang, A. Bauer, H. Berger, C. Pfleiderer, G. van der Laan, and T. Hesjedal, Imaging and manipulation of skyrmion lattice domains in Cu_2OSeO_3, Appl. Phys. Lett. **109**, 192406 (2016).

[45] S. L. Zhang, A. Bauer, D. M. Burn, P. Milde, E. Neuber, L. M. Eng, H. Berger, C. Pfleiderer, G. van der Laan, and T. Hesjedal, Multidomain skyrmion lattice state in Cu_2OSeO_3, Nano Lett. **16**, 3285 (2016).

[46] S. L. Zhang, A. Bauer, H. Berger, C. Pfleiderer, G. van der Laan, and T. Hesjedal, Resonant elastic x-ray scattering from the skyrmion lattice in Cu_2OSeO_3, Phys. Rev. B **93**, 214420 (2016).

[47] S. L. Zhang, G. van der Laan, and T. Hesjedal, Direct experimental determination of spiral spin structures via the dichroism extinction effect in resonant elastic soft x-ray scattering, Phys. Rev. B **96**, 094401 (2017).

[48] S. L. Zhang, W. W. Wang, D. M. Burn, H. Peng, H. Berger, A. Bauer, C. Pfleiderer, G. van der Laan, and T. Hesjedal, Manipulation of skyrmion motion by magnetic field gradients, Nat. Commun. **9**, 2115 (2018).

[49] K. Shibata, J. Iwasaki, N. Kanazawa, S. Aizawa, T. Tanigaki, M. Shirai, T. Nakajima, M. Kubota, M. Kawasaki, H. S. Park, D. Shindo, N. Nagaosa, and Y. Tokura, Large anisotropic deformation of skyrmions in strained crystal, Nat. Nanotechnol. **10**, 589 (2015).

[50] JuMag — A Julia package for classical spin dynamics and micromagnetic simulations with GPU support, https://github.com/ww1g11/JuMag.jl (2019).

[51] M. Beg, R. Carey, W. Wang, D. Cortés-Ortuño, M. Vousden, M.-A. Bisotti, M. Albert, D. Chernyshenko, O. Hovorka, R. L. Stamps, and H. Fangohr, Ground state search, hysteretic behaviour and reversal mechanism of skyrmionic textures in confined helimagnetic nanostructures, Sci. Rep. **5**, 17137 (2015).

[52] O. Janson, I. Rousochatzakis, A. A. Tsirlin, M. Belesi, A. A. Leonov, U. K. Rößler, J. van den Brink, and H. Rosner, The quantum nature of skyrmions and half-skyrmions in Cu_2OSeO_3, Nat. Commun. **5**, 5376 (2014).

[53] D. M. Burn, S. L. Zhang, S. Wang, H. F. Du, G. van der Laan, and T. Hesjedal, Helical magnetic ordering in thin FeGe membranes, Phys. Rev. B **100**, 184403 (2019).

[54] A. Bogdanov and A. Hubert, Thermodynamically stable magnetic vortex states in magnetic crystals, J. Magn. Magn. Mater. **138**, 255 (1994).

[55] A. B. Butenko, A. A. Leonov, U. K. Rößler, and A. N. Bogdanov, Stabilization of skyrmion textures by uniaxial distortions in noncentrosymmetric cubic helimagnets, Phys. Rev. B **82**, 052403 (2010).

[56] J. H. Han, J. Zang, Z. Yang, J. H. Park, and N. Nagaosa, Skyrmion lattice in a two-dimensional chiral magnet, Phys. Rev. B **82**, 094429 (2010).

[57] T. Tanigaki, K. Shibata, N. Kanazawa, X. Yu, Y. Onose, H. S. Park, D. Shindo, and Y. Tokura, Real-space observation of short-period cubic lattice of skyrmions in MnGe, Nano Lett. **15**, 5438 (2015).

[58] H. Wilhelm, M. Baenitz, M. Schmidt, U. K. Rößler, A. A. Leonov, and A. N. Bogdanov, Precursor Phenomena at the Magnetic Ordering of the Cubic Helimagnet FeGe, Phys. Rev. Lett. **107**, 127203 (2011).